

Antiferromagnetism of Ni_2NbBO_6 with $S = 1$ dimer quasi-1D armchair chains

G. Narsinga Rao,¹ Viveka Nand Singh,^{2,3} R. Sankar,¹
I. Panneer Muthuselvan,¹ Guang-Yu Guo,^{3,*} and F. C. Chou^{1,4,5,†}

¹Center for Condensed Matter Sciences, National Taiwan University, Taipei 10617, Taiwan

²Institute of Atomic and Molecular Sciences, Academia Sinica, Taipei 10617, Taiwan

³Department of Physics, National Taiwan University, Taipei 10617, Taiwan

⁴National Synchrotron Radiation Research Center, Hsinchu 30076, Taiwan

⁵Taiwan Consortium of Emergent Crystalline Materials,
Ministry of Science and Technology, Taipei 10622, Taiwan

Long range antiferromagnetic (AFM) ordering of Ni spins in Ni_2NbBO_6 has been studied with single crystal from spin susceptibility measurement and compared with the *ab initio* calculation results consistently. Below $T_N \sim 23.5$ K, the $S = 1$ spins align along the a -direction for edge-shared NiO_6 octahedra which form crystallographic armchair chains along the b -direction. The isothermal magnetization $M(H)$ below T_N shows spin-flop transition for magnetic field above ~ 36 kOe along the a -axis, which indicates the spin anisotropy is along the a -direction. The electronic and magnetic structures of Ni_2NbBO_6 have also been explored theoretically using density functional theory with generalized gradient approximation plus on-site Coulomb interaction (U). These calculations support the experimentally observed antiferromagnetism of Ni_2NbBO_6 . In particular, the long range AFM ordering below T_N can be dissected into armchair chains which consists of $S = 1$ dimers of $J_2 \sim 2.43$ meV with ferromagnetic (FM) intra-chain and inter-chain couplings of size $\lesssim \frac{1}{2}|J_2|$.

PACS numbers: 75.50.Ee, 75.30.Et, 75.30.Gw, 71.15.Mb

I. INTRODUCTION

Low dimensional magnetic materials have attracted considerable attention due to their interesting low temperature properties with the involved strong quantum fluctuations^{1,2}. Extensive studies of materials with geometric frustration on square, triangular, zigzag chains and zigzag ladders spin systems have been explored for the diverse magnetic ground states. The zigzag spin chain of $S = 1/2$ with antiferromagnetic (AFM) interactions between nearest neighbor (NN) and next nearest neighbor (NNN) is about the most commonly studied frustrated system^{3,4}. In zigzag spin chain system with $S = 1$, the ground state phase diagram as a function of anisotropy and ratio between NN and NNN interactions exhibits different phases^{5,6}. Metal borates are expected to be good candidates to serve as links for transition metal polyhedra giving rise to different low-dimensional structures⁷. Another important role of the borate anions, being non-magnetic, is to allow transmission of magnetic interactions via a super-superexchange route^{8–11}.

In the present work, we report the crystal growth and the magnetization measurement results along the three principal directions of Ni_2NbBO_6 . Crystallographically Ni_2NbBO_6 has been found to be a $S = 1$ armchair spin chain system¹². We found that a long range AFM spin ordering exists below $T_N \sim 23.5$ K. A sizable inter-chain coupling leads to the 3D long range AFM spin ordering with an on-site anisotropy along the a -direction, which is as confirmed by the field-induced spin flop transition. We also studied the electronic and magnetic properties of Ni_2NbBO_6 within the density functional theory with the generalized gradient approximation. We found that the system consists of unconventional armchair chains which

are formed with ferromagnetically coupled $S = 1$ dimers with intra- and inter-chain coupling constants which are nearly half of that for the $S = 1$ dimer. An interpretation on the experimental observation on the AFM and spin flop transition is provided and compared with the calculated results.

II. EXPERIMENTAL AND COMPUTATIONAL DETAILS

Single crystal of Ni_2NbBO_6 was grown by a flux method using borate as the solvent. A mixture of 6.6 g NiO , 20 g Nb_2O_5 and 33 g of $\text{Na}_2\text{B}_4\text{O}_7$ were placed in a platinum crucible and heated to 1250°C in a box furnace for 24 hours. The furnace was slowly cooled down to 850°C at a rate of $3^\circ\text{C}/\text{h}$ and then cooled down to room temperature at the rate of $80^\circ\text{C}/\text{h}$. The single crystals in green color (shown in the inset of Fig. 1(b)) were separated from the borate flux by leaching with a dilute solution of HNO_3 . The crystal structure and phase purity of the samples were checked by powder X-ray diffraction (XRD) using the synchrotron X-ray of $\lambda = 0.619$ Å (NSRRC, Taiwan) at room temperature. The field cooled (FC) and zero field cooled (ZFC) magnetization curves were measured in a commercial Vibrating Sample Magnetometer (VSM, Quantum Design, USA) from 1.8 K to 300 K in the presence of various applied magnetic fields. The isothermal magnetization (M) data were also recorded at selected temperatures.

Theoretical calculations have been performed based on first-principle density functional theory (DFT) with generalized gradient approximation (GGA)¹³. The on-site Coulomb energy U has been taken into account using

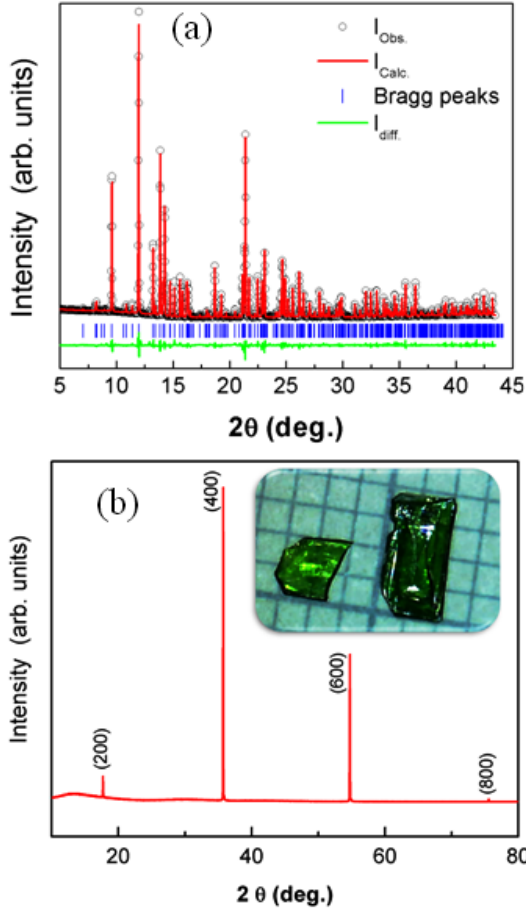


FIG. 1. (Color online) (a) The powder XRD pattern from the pulverized as-grown Ni_2NbBO_6 crystal. (b) The XRD pattern of Ni_2NbBO_6 crystal perpendicular to the large surface to show (h00) peaks with preferred orientation. Inset is the as-grown single crystal.

the GGA+U scheme¹⁴. We have used effective $U_{eff} = (U - J) = 6$ eV for the Ni atoms in the GGA+U calculations. We used the accurate full-potential projector-augmented wave (PAW) method¹⁵ implemented in the Vienna *ab initio* simulation package (VASP)^{16–18}. Experimental lattice parameters were used in the calculation. The primitive unit cell contains four Ni_2NbBO_6 formula units. In the present calculations, we used the tetrahedron method with Blöchl corrections for the Brillouin zone integration with a Γ -centered Monkhorst-Pack k-point mesh of $(8 \times 10 \times 18)$. A large plane wave cutoff energy of 500 eV was taken, and the convergence criterion for the total energy was 10^{-6} eV.

III. RESULTS AND DISCUSSION

A. Crystal structure

The powder XRD pattern of the polycrystalline sample obtained from the pulverized as-grown Ni_2NbBO_6 single

crystal sample is shown in Fig. 1(a). All diffraction peaks can be indexed to the orthorhombic structure with space group Pnma, without any observable trace of impurity phase. The structural parameters were refined by the Rietveld technique with good quality refinement parameters ($R_{wp} = 1.67\%$ and $R_p = 1.04\%$). The obtained values of the lattice parameters are $a = 10.0690(1)$ Å, $b = 8.6266(2)$ Å, and $c = 4.4932(3)$ Å, which are in good agreement with previously reported values¹². Fig. 1(b) illustrates the single crystal XRD pattern with peaks indexed for the preferred orientation perpendicular to the (h00) planes. This compound could also be viewed as layers containing armchair chains of edge-shared NiO_6 octahedra, where each pair of NiO_6 along the b -direction are edge-shared with both NbO_6 octahedra and BO_4 tetrahedra, as illustrated in Fig. 2.

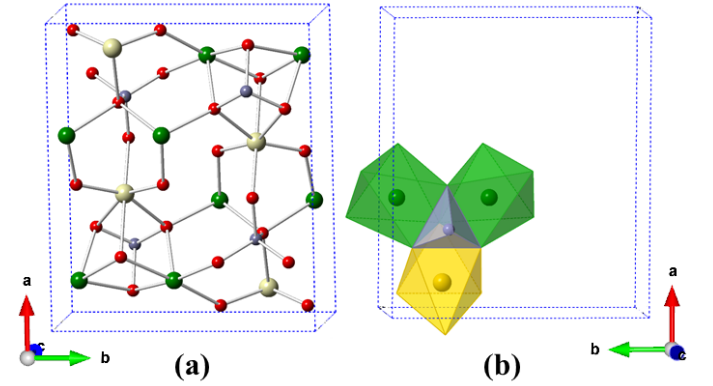


FIG. 2. (Color online) (a) A layer of edge-shared NiO_6 octahedra (green) shown in c -projection containing armchair chains along the b -direction, where every BO_4 tetrahedron (blue) in the neighboring layer bridges a pair of NiO_6 and one NbO_6 octahedra (yellow) through face-sharing, as shown in (b).

B. Magnetic susceptibility

Fig. 3 shows the temperature dependence of magnetic susceptibility $\chi(T)$ and the corresponding inverse susceptibility $\chi^{-1}(T)$ measured at an applied magnetic field of 10 kOe in the temperature range 2–300 K for pulverized powder of the as-grown Ni_2NbBO_6 crystal. The $\chi(T)$ curve shows a Curie-Weiss like behavior at high temperature and a sharp peak is observed at 24 K, indicating the onset of an antiferromagnetic ordering. The ordering temperature $T_N = 23.5$ K is defined by the sharp peak through $d(\chi T)/dT$. At $T > 50$ K, the $\chi(T)$ data can be fitted with the Curie-Weiss law ($\chi(T) = C/(T - \theta)$) satisfactorily using the Curie constant $C = 1.31$ and the Curie-Weiss temperature ($\theta = 9.5$ K), as shown by the red solid line in Fig. 3. The effective moment of $\mu_{eff} = 3.23 \mu_B$ per Ni^{2+} extracted from Curie constant is higher than the expected spin-only value of $\mu_{calc} = 2.83 \mu_B$ for $S = 1$, which suggests the existence of a partially unquenched

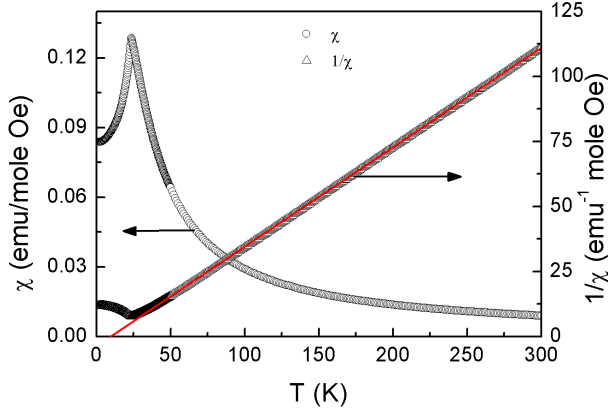


FIG. 3. (Color online) The temperature dependence of magnetic susceptibility $\chi(T)$ and the corresponding inverse susceptibility $\chi^{-1}(T)$ measured at an applied magnetic field of 10 kOe in the temperature range 2 – 300 K for the pulverized as-grown Ni_2NbBO_6 crystals.

orbital contribution. The fitted value of $\theta = 9.5$ K suggests the existence of an average ferromagnetic (FM) coupling among spins at high temperature but AFM ordering occurs at $T_N \sim 23.5$ K, which suggests that the magnetic interactions must consider couplings beyond nearest neighbor spins and have different signs containing both ferromagnetic (FM) and AFM couplings, as verified later by our *ab initio* studies in the following. The $\chi(T)$ data above 200 K were also fitted by high temperature series (HTS) expansion up to 8th order.¹⁹ The fitting parameters are found to be $g = 2.02$ and the exchange interaction $(J/k_B) = -6.6$ K.

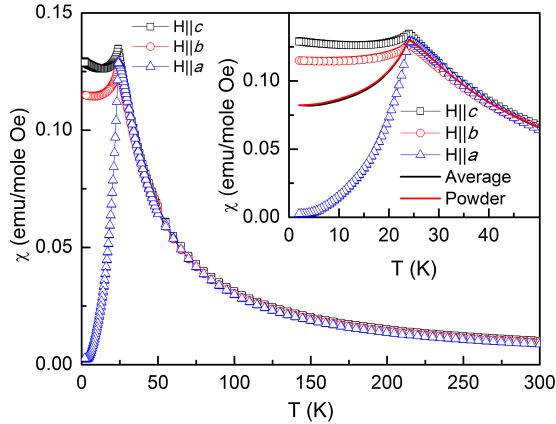


FIG. 4. (Color online) The magnetic susceptibilities $\chi(T)$ for Ni_2NbBO_6 single crystal measured in an applied magnetic field of 10 kOe parallel to all three crystallographic axis. The average of single crystal susceptibility ($\chi(T) = (\chi_a + \chi_b + \chi_c)/3$) agrees perfectly with those measured using powder sample directly.

Anisotropic magnetic susceptibilities $\chi(T)$ for

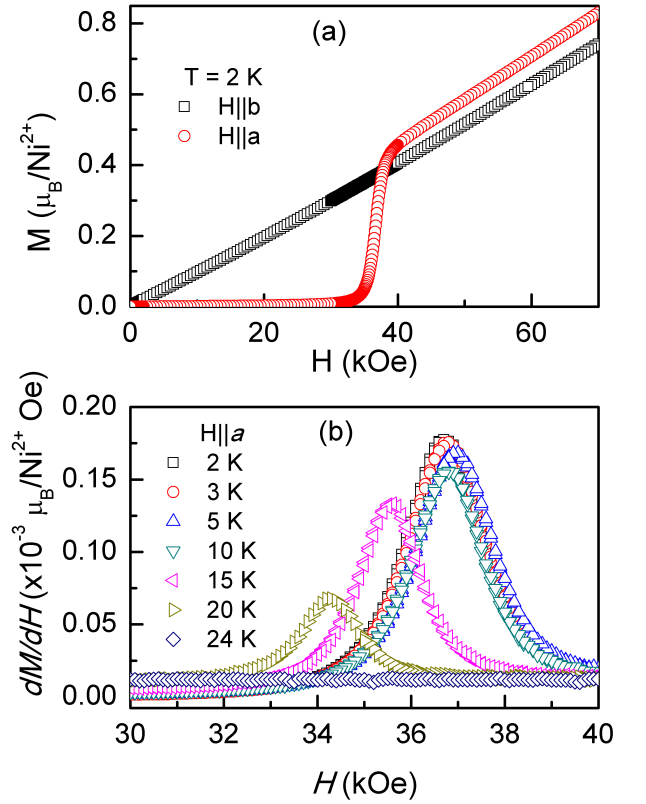


FIG. 5. (Color online) (a) Isothermal magnetization $M(H)$ curves of Ni_2NbBO_6 for the magnetic field parallel to different crystallographic axis (b) dM/dH curves of Ni_2NbBO_6 for the magnetic field parallel to a -axis at some selected temperatures.

Ni_2NbBO_6 single crystals were measured in an applied magnetic field of 10 kOe parallel to all three crystallographic axes, as shown in Fig. 4. There is no deviation between $\chi_{ZFC}(T)$ and $\chi_{FC}(T)$ throughout the measured temperature range. Below T_N , the anisotropy becomes significantly enhanced as shown in the inset of Fig. 4, which indicates that the spins are aligned along the a -axis for in the 3D AFM long range ordering.

To understand the AFM behavior of Ni_2NbBO_6 better, we measured magnetization as a function of magnetic field H along the two crystal orientations above and below T_N , as shown in Fig. 5(a), where no field or temperature hysteresis were observed. For magnetic field parallel to the a -axis, the magnetization reveals jump at a critical field H_C near $H_C = 36.7$ kOe below T_N at 2 K, which is attributed to a spin-flop transition when the spin susceptibility changes abruptly to a higher level, *i.e.*, the ordered spins originally aligned along the a -direction flop to the direction perpendicular to the external field. As expected for the ordered spins aligned along the a -direction, we do not observe spin-flop transition manifested in $M(H)$ for H is applied parallel to b - or c - axis. We may summarize the H - T phase diagram for Ni_2NbBO_6 based on the magnetic field and temperature dependence of $M(T, H)$

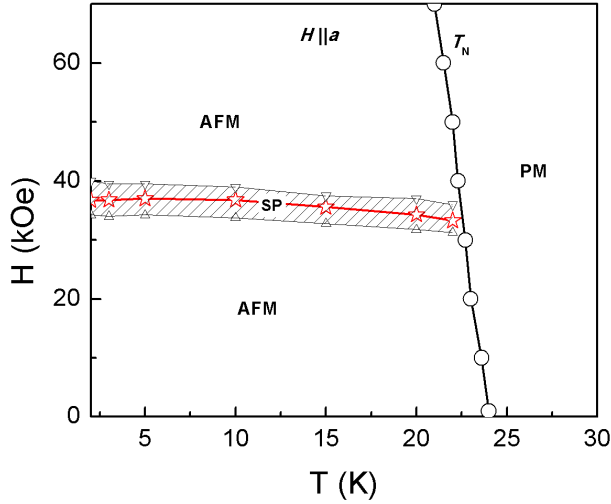


FIG. 6. (Color online) H - T phase diagram of Ni_2NbBO_6 for magnetic field parallel to a -axis obtained from magnetization measurements. The shaded area is related to the spin-flop (SP) transition defined by the start and end points of the transition from $M(T, H)$. Open circles represent measured T_N and solid line is guide to the eye.

with field applied parallel to a -axis, as shown in Fig. 6. A small field dependence of T_N is also shown, where the boundary of spin-flop transition is indicated according to the onsets of dM/dH peaks shown in Fig. 5(b).

C. Theoretical calculations

Within first-principle density functional theory, we first calculated the total energy (E_{FM}) for the ferromagnetic state. The total energy per formula unit (f.u.) is -72.7578 eV. In order to find out the magnetic ground state of the system, we have considered various magnetic configurations possible within the unit cell. Three configurations corresponding to the possible magnetic ground states have been used to estimate the exchange interactions, and three coupling constants (J_i) are considered based on the three shortest Ni-Ni distances, as shown in Fig. 7. Here J_1 , J_2 , and J_3 represent the exchange couplings between two neighboring Ni atoms corresponding to the Ni-Ni distances of 2.987 Å, 3.099 Å, and 3.436 Å, respectively, as shown in Fig. 7. Both ferromagnetic as well as antiferromagnetic alignments of Ni spins are considered and labelled as configurations A, B, and C. The calculated total energies of all these configurations are summarized in Table I.

We find that the configuration A (Fig. 7) has the lowest energy, therefore configuration A is the expected magnetic ground state of the system. In this configuration, all the NN Ni ions within the armchair chain along the b -direction are antiferromagnetically coupled as a $S = 1$ dimer, and the other two NNN Ni ions, *i.e.*, the interdimer within the armchair chain and the inter-chain cou-

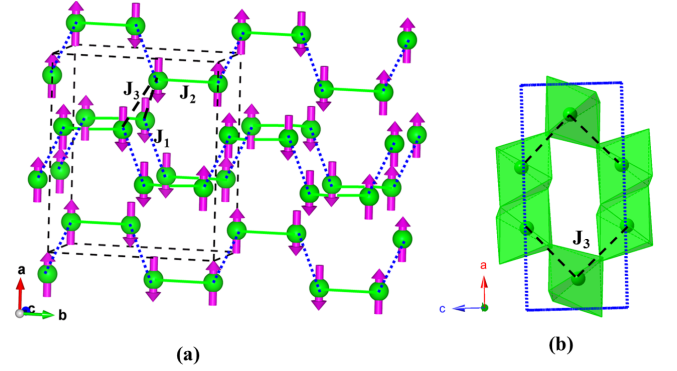


FIG. 7. (Color online) A schematic representation of the spin arrangement for configuration A.

plings are ferromagnetically coupled.

The calculated magnetic moment of Ni is $\sim 1.78 \mu_B$, which is slightly smaller than the expected value of $2 \mu_B$ for Ni^{2+} , suggesting that some of the magnetic moment lies outside the nickel atomic sphere used. Fig. 8 shows the band structure (top panel) and density of states (bottom panel) of configuration A. We find that the system has a large gap $\gtrsim 3$ eV, which indicates that the system is insulating and consistent with the experimental observation. It is quite clear from the site-resolved density of states that the valence band is mainly composed of nickel 3d and oxygen 2p states. Thus the magnetic structure should be primarily decided by the spin-exchange coupling via Ni-O-Ni.

Next we evaluated the intra-chain and inter-chain magnetic exchange couplings among Ni spins. The exchange interaction between all the nearest-neighbor Ni ions along the b -direction in the ab -plane is denoted as J_2 , and the other two couplings are J_1 (intra-chain) and J_3 (inter-chain), as illustrated in Fig. 7. In order to evaluate the exchange couplings, we have considered the obtained total energy of the unit cell of Ni_2NbBO_6 as the sum of the nearest-neighbor spin-spin interactions in terms of the spin Heisenberg model $H = E_0 + \sum_{\langle ij \rangle} J_{ij} \sigma_i \cdot \sigma_j$. Here J_{ij} is the exchange interaction parameter between the nearest-neighbor Ni site i and site j , and σ_i (σ_j) is the unit vector representing the direction of the local magnetic moment at site i (j). The total energy per unit cell

TABLE I. Calculated total energy ΔE (relative to the total energy of FM state $E_{FM} = 72.7578$ eV/f.u.), total magnetic moment m_s^{tot} , atomic moment of Ni m_s^{Ni} and band gap E_g

Config.	ΔE (meV/f.u.)	m_s^{tot} (μ_B /f.u.)	m_s^{Ni} (μ_B /atom)	E_g (eV)
FM	0.0	4.0	1.78	2.9
A	-4.87	0.0	1.78	3.3
B	-2.0	0.0	1.78	3.3
C	-2.16	0.0	1.78	3.3

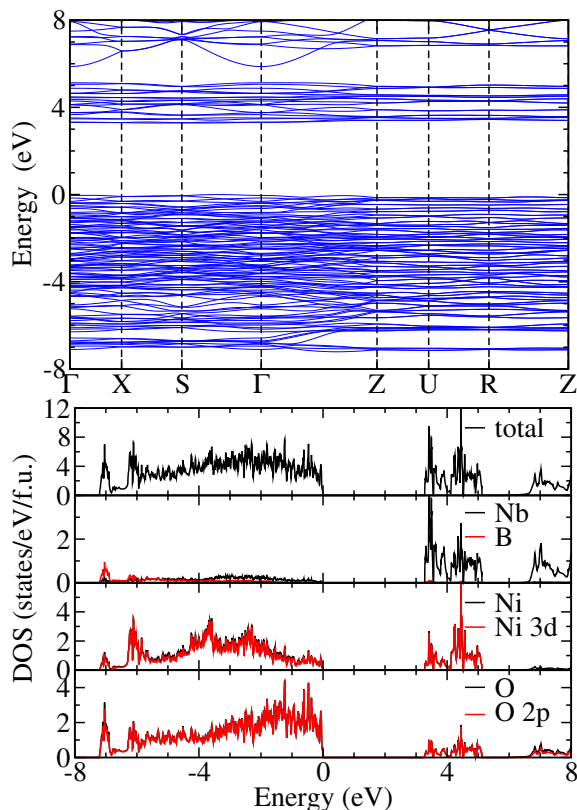


FIG. 8. (Color online) Band structure (top panel) and density of states (bottom panel) of configuration A. Top of the valence band has been set to zero.

TABLE II. Calculated exchange interaction parameters (J_i) and the corresponding nearest-neighbor Ni-Ni distances.

	J_1	J_2	J_3
J_i (meV)	-1.43	2.43	-1.27
Ni-Ni(Å)	2.987	3.099	3.436

for all considered magnetic configurations are given by

$E_{FM} = E_0 + 4(J_3 + J_1) + 4J_2$, $E_A = E_0 + 4(J_3 + J_1) - 4J_2$, $E_B = E_0 + 4(J_3 - J_1) - 4J_2$, and $E_C = E_0 - 4J_2$. Solving the above mentioned equations we get the values of all exchange interactions listed in Table II, where $J > 0$ for AFM interaction and $J < 0$ for FM interaction, and the constant E_0 contains all spin-independent interactions. Although the Ni-Ni distances for all these FM and AFM couplings are very close, the strength of the AFM coupling is nearly twice of the FM coupling, which could be due to the strong bonding of boron tetrahedra that bridge the NiO_6 pairs within each armchair chain. The AFM superexchange coupling has the largest magnitude of 2.43 meV, which roughly corresponds to $T_N \sim 28$ K and in good agreement with the experimental observation of $T_N \sim 23.5$ K.

IV. SUMMARY

The magnetic properties of Ni_2NbBO_6 containing armchair chains have been studied in detail through $M(H, T)$ measurement of the single crystal sample and compare with models predicted by the *ab initio* calculations. A long range AFM spin ordering observed below $T_N \sim 23.5$ K. The spin-flop transition of critical field 36.7 kOe at 2 K is found along *a*-axis and the *H-T* phase diagram is constructed accordingly. Within first-principle density functional theory, we have calculated the electronic and magnetic structures with exchange interactions that agree satisfactorily with the experimental results. We have established that Ni_2NbBO_6 consists of unusual armchair chains which are formed with $S = 1$ dimers with ferromagnetic intra- and inter-chain couplings.

V. ACKNOWLEDGEMENT

FCC acknowledges the support provided by MOST-Taiwan under project number MOST 102-2119-M-002-004. GYG acknowledges the financial support for this work from the Academia Sinica Thematic Research Program and the Ministry of Science and Technology of Taiwan.

* gyguo@phys.ntu.edu.tw

† fcchou@ntu.edu.tw

¹ H. T. Diep, "Magnetic systems with competing interactions (Frustrated spin systems)", World Scientific, Singapore, 1994.

² M. Troyer, H. Tsunetsugu and D. Wurtz, Phys. Rev. B **50**, 13515 (1994).

³ S. R. White and I. Affleck, Phys. Rev. B **54**, 9862 (1996).

⁴ M. Matsuda and K. Katsumata, J. Magn. Magn. Mater. **140-144**, 1671 (1995).

⁵ T. Hikihara, M. Kaburagi, H. Kawamura and T. Tonegawa, J. Phys. Soc. Japan **69**, 259 (2000).

⁶ A. Kolezhuk, R. Roth and U. Schollwock, Phys. Rev. Lett. **77**, 5142 (1996).

⁷ J. D. Grice, P. C. Burns and F. C. Hawthorne, Can. Mineral. **37**, 731 (1999).

⁸ V. V. Grishachev, O. S. Kolotov, A. P. Krasnojon and V. A. Pogozhev, J. Magn. Magn. Mater. **241**, 81 (2002).

⁹ J. P. Attfield, A. M. T. Bell, L. M. Rodriguez-Martinez, J.M.Greeneche, R. J. Cernik, J. F. Clarke and D. A. Perkins, Nature **396**, 655 (1998).

¹⁰ J. C. Fernandes, F. S. Sarrat, R. B. Guimaraes, R. S. Freitas, M. A. Continentino, A. C. Doriguetto, Y. P. Mascarenhas, J. Ellena, E. E. Castellano, J-L. Tholence, J. Dumas, and L. Ghivelder, Phys. Rev. B **67**, 104413 (2003).

- ¹¹ J. C. Fernandes, R. B. Guimaraes, M. A. Continentino, R. Rapp, J-L. Tholence, J. Dumas, Y. Blancquaert, S. Yates, and C. Paulsen, Phys. Rev. B **69**, 054418 (2004).
- ¹² G. B. Ansell, M. E. Leonowicz, M. A. Modrick, B. M. Wanklyn and F. R. Wondre, Acta Cryst. B **38**, 892 (1982).
- ¹³ J. P. Perdew, K. Burke and M. Ernzerhof, Phys. Rev. Lett. **77**, 3865 (1996).
- ¹⁴ S. L. Dudarev, G. A. Botton, S. Y. Savrasov, C. J. Humphreys and A. P. Sutton, Phys. Rev. B **57**, 1505 (1998).
- ¹⁵ P. E. Blöchl, Phys. Rev. B **50**, 17953 (1994).
- ¹⁶ G. Kresse and J. Hafner, Phys. Rev. B **47**, 558 (1993); **49**, 14251 (1994).
- ¹⁷ G. Kresse and J. Furthmüller, Comput. Mater. Sci. **6**, 15 (1996).
- ¹⁸ G. Kresse and D. Joubert, Phys. Rev. B **59**, 1758 (1999).
- ¹⁹ G. S. Rushbooke and P. J. Wood, J. Molec. Phys. **1**, 257 (1958).